Published online 3 July 2018

Nucleic Acids Research, 2018, Vol. 46, No. 17 ***8817–8831***
doi: 10.1093/nar/gky585

H2A.Z.1 crosstalk with H3K56-acetylation controls gliogenesis through the transcription of folate receptor

Libo Su[1,2], Wenlong Xia[1,3], Tianjin Shen[1,2], Qingli Liang[1,2], Wenwen Wang[1,3], Hong Li[1,2] and Jianwei Jiao[1,2,*]

[1]State Key Laboratory of Stem Cell and Reproductive Biology, Institute of Zoology, Chinese Academy of Sciences, Beijing 100101, China, [2]University of Chinese Academy of Sciences, Beijing 100049, China and [3]School of Life Sciences, University of Science and Technology of China, Hefei 230026, China

Received February 28, 2018; Revised June 10, 2018; Editorial Decision June 17, 2018; Accepted June 18, 2018

ABSTRACT

Astrocytes play crucial roles in the central nervous system, and defects in astrocyte function are closely related to many neurological disorders. Studying the mechanism of gliogenesis has important implications for understanding and treating brain diseases. Epigenetic regulations have essential roles during mammalian brain development. Here, we demonstrate that histone H2A.Z.1 is necessary for the specification of multiple neural precursor cells (NPCs) and has specialized functions that regulate gliogenesis. Depletion of *H2A.Z.1* suppresses gliogenesis and results in reduced astrocyte differentiation. Additionally, H2A.Z.1 regulates the acetylation of H3K56 (H3K56ac) by cooperating with the chaperone of ASF1a. Furthermore, RNA-seq data indicate that folate receptor 1 (FOLR1) participates in gliogenesis through the JAK–STAT signaling pathway. Taken together, our results demonstrate that H2A.Z.1 is a key regulator of gliogenesis because it interacts with ASF1a to regulate H3K56ac and then directly affects the expression of FOLR1, which acts as a signal-transducing component of the JAK–STAT signaling pathway.

INTRODUCTION

During brain development, neurons are generated during early stages and glial cells, including astrocytes and oligodendrocytes, are produced during later stages. The sequential appearance of neurons and glia in the vertebrate central nervous system is very important to the embryonic cortex development. The neurogenesis and gliogenesis are related with each other, but they also have differences (1–3). Among these cells, astrocytes are the most abundant type and are mainly derived from NPCs in the subventricular zone (SVZ) of the perinatal brain (4,5). Increasing evidence indicates that astrocytes perform diverse functions, such as maintaining the neural microenvironment, protecting the blood-brain barrier (BBB), regulating cerebral blood flow, and participating in synapse formation (6–10). The process of astrocyte formation, which is also referred to as astrocytogenesis, is associated with many signaling cascades. Among them, the cytokine-induced JAK -STAT signaling pathway plays a critical role in the control of gliogenesis (11–13). Cytokines, including leukemia inhibitory factor (LIF) and ciliary neurotrophic factor (CNTF), use gp130 as a signal-transducing component in their receptor complexes to induce differentiation of astrocytes (14–16). Additionally, understanding the molecular mechanism of gliogenesis will be beneficial to the treatment of glial-related disease such as glioma and Alzheimer's disease (17,18).

Histone H2A.Z.1 is one of the most evolutionarily conserved variants of H2A and is a key epigenetic regulatory factor that is associated with a wide variety of biological processes (19). In vertebrates, H2A.Z.1 is encoded by the *H2AFZ* gene, significantly differs from H2A in the C terminus and contains a short region (20). Previous work indicates that H2A.Z.1 is involved in multiple epigenetic and transcriptional events, such as heterochromatin formation, chromosome segregation, mitosis and gene transcription regulation (21–23). Consistent with these functions, H2A.Z.1 has been found to be located in the promoter regions of genes and is associated with other regulatory regions (24,25). Recently, H2A.Z.1 has been found to have specialized functions that regulate lineage commitment during cellular specification and regulated embryonic neurogenesis by targeting *Nkx2-4* through interaction with Setd2 (26,27), which suggests that H2A.Z.1 may be necessary for the specification of NPCs in the central nervous system (CNS). As for the embryonic cortex development, neurogenesis and gliogenesis are inextricably intertwined. How-

*To whom correspondence should be addressed. Tel: +86 10 64806335; Email: jwjiao@ioz.ac.cn

ever, whether H2A.Z.1 regulates gliogenesis remains largely unexplored. Connecting neurogenesis and gliogenesis will provide a framework for understanding how disruption in the H2A.Z.1 may contribute to neurological disorders. A variety of covalent modifications in histones variants, including acetylation and methylation, which together with epigenetic factors play essential roles in brain development (28). Among these modifications, acetylation at lysine 56 of histone H3 (H3K56ac) is abundant at transcriptional start sites (TSS) of genes and functions in replication-coupled nucleosome assembly and chromatin disassembly during transcriptional activation (29–31). As a recently demonstrated and relatively unstudied chromatin marker in mammalian cells (32), H3K56ac not only regulates gene transcriptional activation but is also related to memory formation in the hippocampus (33). Whether there is a connection between H2A.Z.1 and H3K56ac in the regulation of the developing cortex remains largely unknown.

Folate receptor 1 (FOLR1) is a folic acid transporter that is located on the cell surface due to a glycophosphatidylinositol (GPI)-anchor (34). The major function of FOLR1 is transporting folic acid into cells, and we found that FOLR1 is associated with the JAK–STAT signaling pathway. In this study, we focus on the function of H2A.Z.1 in the later stages of cerebral cortex development. To achieve this goal, we performed *in utero* electroporation of H2A.Z.1 shRNAs and a conditional knockout of the *H2AFZ* gene in progenitors of the astrocyte lineage. The results demonstrated that *H2A.Z.1* deletion disrupts glial progenitor specification into astrocytes and impairs gliogenic signaling during astrocyte development. To explore the mechanisms of astrocytogenesis defects, we conducted a series of *in vivo* and *in vitro* experiments. The results revealed that H2A.Z.1 interacts with a chaperone of histones (ASF1a) to regulate H3K56ac at the core promoter regions of the *Folr1* gene. Additionally, FOLR1 participates in gliogenesis through the JAK–STAT signaling pathway. Finally, our work provides a critical foundation for H2A.Z.1 as a regulator of astrocyte fate determination, and the control of H2A.Z.1 dynamics is critical for the regulation of gliogenesis during brain development.

MATERIALS AND METHODS

Genetically modified mice

We used the following mouse strains: *H2A.Z.1*^{flox} (RIKEN # RBRC 05765: B6.Cg-H2az.1$^{tm1.1Hko}$), *hGFAP-Cre* (JAX stock # 004600) (35), *Nestin-Cre* mice (B6. Cg-Tg(Nes-cre)1Kln/J). The H2A.Z.1 floxed mice were provided by the RIKEN BRC through the National Bio-Resource Project of the MEXT. ICR (Institute of Cancer Research) pregnant female mice were used for in utero electroporation.

H2A.Z.1^{cKO} mice were generated from *H2A.Z.1*$^{fl/fl}$ females which carrying the loxP-flanked alleles and *hGFAP-Cre* males which carrying the Cre alleles. All mice were housed on a 12 h dark/light cycle with the standard rodent chow. All laboratory animal procedures were approved by the Animal Care and Use Committee of Institute of Zoology, Chinese Academy of Sciences, China.

In utero and postnatal electroporation

The protocols of *in utero* electroporation have been previously described (36). Briefly, timed-pregnant ICR female mice or *H2A.Z.1*^{cKO} mice were anesthetized using 0.07% (w/v) Pentobarbital Sodium and embryos were exposed. Recombinant plasmid mixed with enhanced GFP plasmid (Venus-GFP) at a 3:1 ratio and 0.02% (w/v) fast green (Sigma). The mixed plasmid was gently microinjected into the fetal lateral ventricles with paddle electrodes. Using an electroporator (ECM80, Manual BTX), every embryo was electroporated with five 50 ms pulses at 45 V with 950 ms interval. Subsequently, the uterine horns were gently returned to the abdominal cavity. For postnatal electroporation, 1 ul of recombinant plasmid DNA was injected into the lateral ventricles and three 100-ms pulses at 100 V with a 950-ms interval were administered. Brains were dissected and fixed in 4% PFA at 4°C overnight and then dehydrated in 30% (w/v) sucrose at 4°C. Using a cryostat microtome (Leica CM1950), brains were cryosectioned at 15 μm and cryoprotected at −80°C.

Cell cultures

HEK293FT (human embryonic kidney cells) and Neuro-2A cell lines were cultured in DMED medium (Life Technologies) supplemented with 10% FBS (nvitrogen), GlutaMAX (0.5%, Invitrogen), nonessential amino acids (NEAA, 1%, Invitrogen) and P/S (1%, Invitrogen).

Lentiviral DNA and the core DNA was transfected into HEK293FT cells by GenEscort^{MT}I (Wisegen, Nanjing). The medium containing virus was harvested at 24, 48 and 72 h post-transfection. To eliminate cell debris, the medium was centrifuged at 3000 rpm for 5 min. The collected virus used to infect NPCs.

E16.5 NPCs were isolated from pregnant ICR mice cortex. The NPCs were seeded into six-well plate and the plates were coated with poly-D-lysine (10 μg/ml, Sigma) and laminin (10 μg/ml, Sigma). For NPCs proliferation and differentiation, the proliferation medium consisted of 50% DMEM/F12 (Invitrogen), 50% NeuroBasal-A medium (Invitrogen), 1% nonessential amino acids (Invitrogen), 0.5% GlutaMax (Invitrogen), 1% P/S (Invitrogen), 2% B27 supplement (Invitrogen) with basic fibroblast growth factor (bFGF, 10 ng/ml, Invitrogen) and epidermal growth factor (EGF, 10 ng/ml, Invitrogen). The NPCs were infected with lentivirus for 12 h by adding polybrene (2 μg/ml) to improve the efficiency of infection. And then, the proliferation medium was changed into glial differentiation medium, which consisted of low-glucose DMEM medium (Gibco) supplemented with 1% FBS, 2% B27 supplement, and 1% P/S. For LIF (Millipore) stimulation experiments, cells were pre-treated for overnight with serum-free DMED medium and treated with LIF (50 ng/ml, Millipore) for 15 min as indicated to analyze the levels of pSTAT3.

Western blotting and co-immunoprecipitation

The transfected cells/tissues were lysed in RIPA buffer (Solarbio) with protease inhibitor (10 mM PMSF and cocktail) on ice for 5 min. The lysates were loaded onto 12% SDS-PAGE gels, and the proteins were transferred to nitrocel-

lulose (NC) membranes. Membranes were blocked in 5% non-fat milk in PBST with 0.1% Tween-20 for 1 h at room temperature and incubated with primary antibodies at 4°C overnight. The gray density of bands was measured by the Odyssey software.

For co-immunoprecipitation, the fresh cell lysates were centrifuged for 10 min at 4°C. Extracts were incubated with anti-HA-tag magnetic beads (MBL) and the same sample was incubated with anti-IgG magnetic beads for negative control at 4°C overnight. After that, the immunoprecipitates were washed by pre-cold washing buffer three times. The magnetic beads complex was suspended with 1× protein loading buffer, and boiled for 2 min. Load 10% protein sample per lane in SDS-PAGE gel.

BrdU labeling

BrdU (100 mg/kg) was administered to pregnant female mice for 2 h before collecting the brains. Then, the brain slices were stained with anti-BrdU antibodies for analysis.

Immunostaining

Immunohistochemistry (IHC) procedure was previously described (37). Briefly, brain cryosections (15 μm) were washed with 1 M phosphate buffer saline (PBS), fixed with 4% paraformaldehyde (PFA) for 20 min at room temperature (RT), and washed three times with PBST (1% Triton X-100 in 1 M PBS) for 15 min. Next, the brain sections were blocked with 5% BSA in PBST (1% Triton X-100 in 1 M PBS) at room temperature for 1 h. And then, the brain slices were incubated in primary antibodies overnight at 4°C and in secondary antibodies at room temperature (RT) for 2 h. After washing, the slices were incubated with DAPI and mounted. For immunocytochemistry, the cells were washed with 1 M phosphate buffer saline (PBS), fixed in 4% paraformaldehyde (PFA), blocked in 5% BSA in PBST (1% Triton X-100 in 1 M PBS) at room temperature for 1 h, incubated with primary antibodies overnight at 4°C and then with secondary antibodies at room temperature (RT) for 2 h.

Antibodies

Immunostaining was performed with the following primary antibodies: H2A.Z.1 (Active-Motif, # 39943, Rabbit, 1:2000), GFAP (Sigma, G6171, Mouse, 1:10 000; Dako, Z033429, Rabbit, 1:3000), Acsbg1 (Abcam, ab 118154, Mouse, 1:1000), Aldh1l1 (Abcam, ab56777, Rabbit, 1:500), GLAST (Proteintech, 20785-1-AP, Rabbit, 1:1000), BLBP (Proteintech, 14836-1-AP, Rabbit, 1:000), S100β (Proteintech, 15146-1-AP, Rabbit, 1:500), Pax6 (Abcam, ab5790, Rabbit, 1:000), Sox2 (R&D,MAB2018, Mouse, 1:1000), BrdU (Abcam, ab6326, Rat, 1:1000), TUJ1 (Millipore, MAB1637, Rabbit, 1:2000), STAT3 (Cell Signaling Technology, 4904P, Mouse, 1:2000), phospho-STAT3 (Tyr705) (Cell Signaling Technology, 9145S, Rabbit, 1:500), β-Actin (Proteintech, 20536-1-AP, Rabbit, 1:5000), Flag (Sigma, F7425, Mouse, 1:2000), H2A (Proteintech, 10445-1-AP, Rabbit, 1:000), H3 (Cell Signaling Technology, 4499, Rabbit, 1:2000), H3K56ac (Abcam, ab76307, Rabbit, 1:2000), H3K9ac (Millipore, 07-352, Rabbit, 1:2000), H3K27ac (Millipore, 07-360, Rabbit, 1:2000), H3K4me3 (Millipore, 07-473, Rabbit, 1:2000), Tri-Methyl-Histone H3 (Lys36) (Cell Signaling Technology, # 9763, Rabbit, 1:2000), FOLR1 (Bioworld Technology, BS3861, Rabbit, 1:500).

Cell cycle analysis by flow cytometry

E16.5 NPCs were isolated from pregnant ICR mice cortex. The NPCs were infected with lentivirus for 12 h, and harvested after 72 h. And then, the cells fixed with 70% ethanol for 4 h at 4°C. Analysis of the cell cycle phases was performed with propidium iodide (50 g/ml, containing 100 g/ml RNase A) staining and analyzed by FACSCalibur cytometer (Becton Dickinson) according to the manufacturer's instructions.

Apoptosis assay

Apoptotic cells were assessed by TUNEL assay using the In Situ Cell Death Detection Kit-TMR Red (Roche) according to manufacturer's protocol.

RT and real-time PCR analysis

The total RNA samples were extracted using TRIzol reagent (Invitrogen) following the manufacturer's instructions. The first-strand cDNA synthesis was performed with the FastQuant RT Kit (with DNase; Tiangen) following the manufacturer's instructions. Real-time PCR analysis was performed using a SYBR qPCR master mix (Tiangen) and signals were detected with the ABI7500 real-time PCR system (Applied Biosystems). All PCR reactions were performed at least in three independent biological repeats. β-Actin used for normalization of qPCR reactions. Related primers (forward sequence and reverse sequence) used for real-time PCR were listed in Supplementary Table S1.

RNA-seq and data analysis

The VZ–SVZ regions were dissected separately from E16.5 and the total RNA dissolved using TRIzol reagent (Invitrogen) following the manufacturer's instructions. RNA-seq was performed by Shanghai Biotechnology Corporation. For data analysis, sequencing reads were disposed by Shanghai Biotechnology Corporation. The scatter plotting and differential gene expression analysis were performed with Cuffdiff and R as previously described (38).

Chromatin immunoprecipitation assays

NPCs were were isolated from E16.5 mice brains cortex and cultured for 3 days in differentiation medium. The cells were crosslinked with 1% formaldehyde/PBS at RT for 15 min. The crosslinking reaction was terminated by addition of 2.5 M glycine. Cells were washed three times with ice-cold PBS, and then collected in lysis buffer 1 (50 mM HEPES–KOH, pH 7.5, 140 mM NaCl, 1 mM EDTA, 10% glycerol, 0.5% NP-40, 0.25% Triton, and protease inhibitor). The cells were washed three times with lysis buffer 2 (10 mM Tris–HCl, pH 8.0, 200 mM NaCl, 1 mM EDTA, 0.5

mM EGTA, and protease inhibitor). After that, the cells were resuspended in lysis buffer 3 (10 mM Tris–HCl, pH 8.0, 100 mM NaCl, 1 mM EDTA, 0.5 mM EGTA, 0.1% sodium deoxycholate, and protease inhibitor). The samples were then sonicated to generate DNA fragments of approximately 0.3 kb. The fragments were then incubated with anti-HA-tag magnetic beads or with normal mouse IgG overnight at 4°C. The last beads were isolated and washed consecutively with washing buffer (0.1% SDS, 1% Triton X-100, 2 mM EDTA, 20 mM Tris–HCl pH 8.0 and 500 mM NaCl) for six times. Immunocomplexes were eluted from the beads with TES buffer (50 mM Tris–HCl pH 8.0, 10 mM EDTA and 1% SDS) overnight at 65°C. Proteins were eliminated by digestion with proteinase K and DNA was purified by TIANamp Genomic DNA Kit (Tiangen). The eluted DNA was subjected to Real-time PCR using a SYBR qPCR master mix (Tiangen) and signals were detected with the ABI7500 real-time PCR system (Applied Biosystems). Related primers (forward sequence and reverse sequence) used for ChIP-qPCR were listed in Supplementary Table S1.

Imaging and statistical analysis

All the Confocal images were achieved through Zeiss LSM780 and analyzed with Photoshop CS6 (Adobe). Quantitative data are presented as means ± S.E.M. The data were analyzed with the two-tailed unpaired Student's *t*-test. For multiple comparisons, the data were analyzed with ANOVAs. $*P < 0.05$, $**P < 0.01$, $***P < 0.001$. All statistical analyses were performed using GraphPad Prism5.0.

RESULTS

H2A.Z.1 expression is closely associated with astrocyte development

To study the function and mechanism of H2A.Z.1 in the developing cortex, we first examined the correlation of H2A.Z.1 expression and cortical development. The expression pattern of H2A.Z.1 in different stages from embryonic day (E) 16 to postnatal day (P) 8 was examined with immunostaining experiments. H2A.Z.1 was strongly present in the ventricular zone (VZ), the subventricular zone (SVZ) and the cortical plate (CP). The astrocyte marker GFAP was also observed in the VZ/SVZ (Figure 1A and B). Furthermore, qPCR analysis validated the expression patterns of H2A.Z.1 and astrocyte markers Aldh1l1, Acsbg1 and GFAP (Supplementary Figure S1A–D). We also performed co-staining experiments and the immunostaining results revealed that H2A.Z.1 co-localized with neuronal maker TUJ1, astrocyte marker GFAP and oligodendrocyte maker MBP (Supplementary Figure S1E). Moreover, we examined H2A.Z.1 expression in cell culture. The immunostaining results revealed that H2A.Z.1 co-localized with SOX2 and NESTIN, which label NPCs *in vitro*. Furthermore, H2A.Z.1 was co-localized with GFAP, Acsbg1 and TUJ1 in the differentiated cells of the neuronal lineage (Figure 1C and Supplementary Figure S1F). Taken together, these results indicate that H2A.Z.1 is dominantly expressed in the CNS, and its expression patterns *in vivo* and *in vitro* indicate a strong relationship between H2A.Z.1 expression and gliogenesis during cerebral cortex development.

H2A.Z.1 regulates gliogenesis during cortical development

Given that H2A.Z.1 expression closely correlates with gliogenesis, we performed a series of experiments to study the function of H2A.Z.1 in regulating astrocyte differentiation. First, we confirmed the two distinct H2A.Z isoforms by qPCR (Supplementary Figure S2C). And then, we generated two different *H2A.Z.1*-specific shRNAs. The knockdown efficiencies were subsequently examined using western blot (Figure 1D). We also used qPCR to confirm the knockdown efficiencies (Supplementary Figure S2A). The *H2A.Z.1*-specific shRNAs efficiently silenced H2A.Z.1 expression in the NPCs with no effect to the silence of H2A.Z.2.1 (Supplementary Figure S2A and B). Second, E16.5 NPCs were infected with control shRNAs or H2A.Z.1-shRNAs lentivirus. Western blot analyses were performed using the different astrocyte makers Aldh1l1 (39), Acsbg1 and GFAP (Figure 1D and E). These data indicated that *H2A.Z.1* knockdown impaired astrocyte differentiation from the glial progenitors. We also generated two different *H2A.Z.2.1*-specific shRNAs and the E16.5 NPCs were infected with control shRNAs or H2A.Z.2.1-shRNAs lentivirus. qPCR analysis of relative mRNA abundance for *GFAP* and *H2AFV* (Supplementary Figure S2D). The results showed that *H2A.Z.2.1* knockdown not impaired astrocyte differentiation. We next performed *in utero* electroporation of plasmids in the lateral ventricles of embryos at E15.5. In the control cortex, most of the GFP^+ cells differentiated into astrocytes that were positive for GFAP from the NPCs, while *H2A.Z.1* knockdown resulted in a dramatic reduction in astrocytes (Figure 1F and G). Then, we investigated whether H2A.Z.1 depleted cells have a block in cell cycle progression. We performed cell cycle analysis by flow cytometry. These data indicated that no significant difference was observed between the percentage of control-shRNA and H2A.Z.1-shRNA in G1 phase (Supplementary Figure S2E). We also investigated the changes of NPCs which labeled by Sox2 and results showed that the number of Sox2-labeled NPCs among the GFP-positive cells was increased (Supplementary Figure S2F and G). Based on the observation that *H2A.Z.1* knockdown *in vivo* disrupted glial progenitor specification in the cortex, we further analyzed *H2A.Z.1* knockdown *in vitro*. Compared with the control, knockdown of *H2A.Z.1* decreased the percentage of $GFAP^+$ astrocytes among the GFP-positive cells (Figure 1H and I). We also performed a terminal deoxynucleotidyltransferase-mediated dUTP end-labeling (TUNEL) assay to assess cells apoptosis. No significant difference was observed between the control and the *H2A.Z.1* knockdown cortex (Supplementary Figure S2H). Overall, both *in vivo* and *in vitro* results revealed that astrocyte differentiation was affected by *H2A.Z.1* knockdown.

Given the observation of reduced astrocyte differentiation due to *H2A.Z.1* knockdown, we performed H2A.Z.1 gain-of-function experiments to further analyze the function of H2A.Z.1 in gliogenesis. Overexpression of H2A.Z.1 significantly promoted gliogenesis and increased the expression of Acsbg1 and GFAP (Supplementary Figure S2I

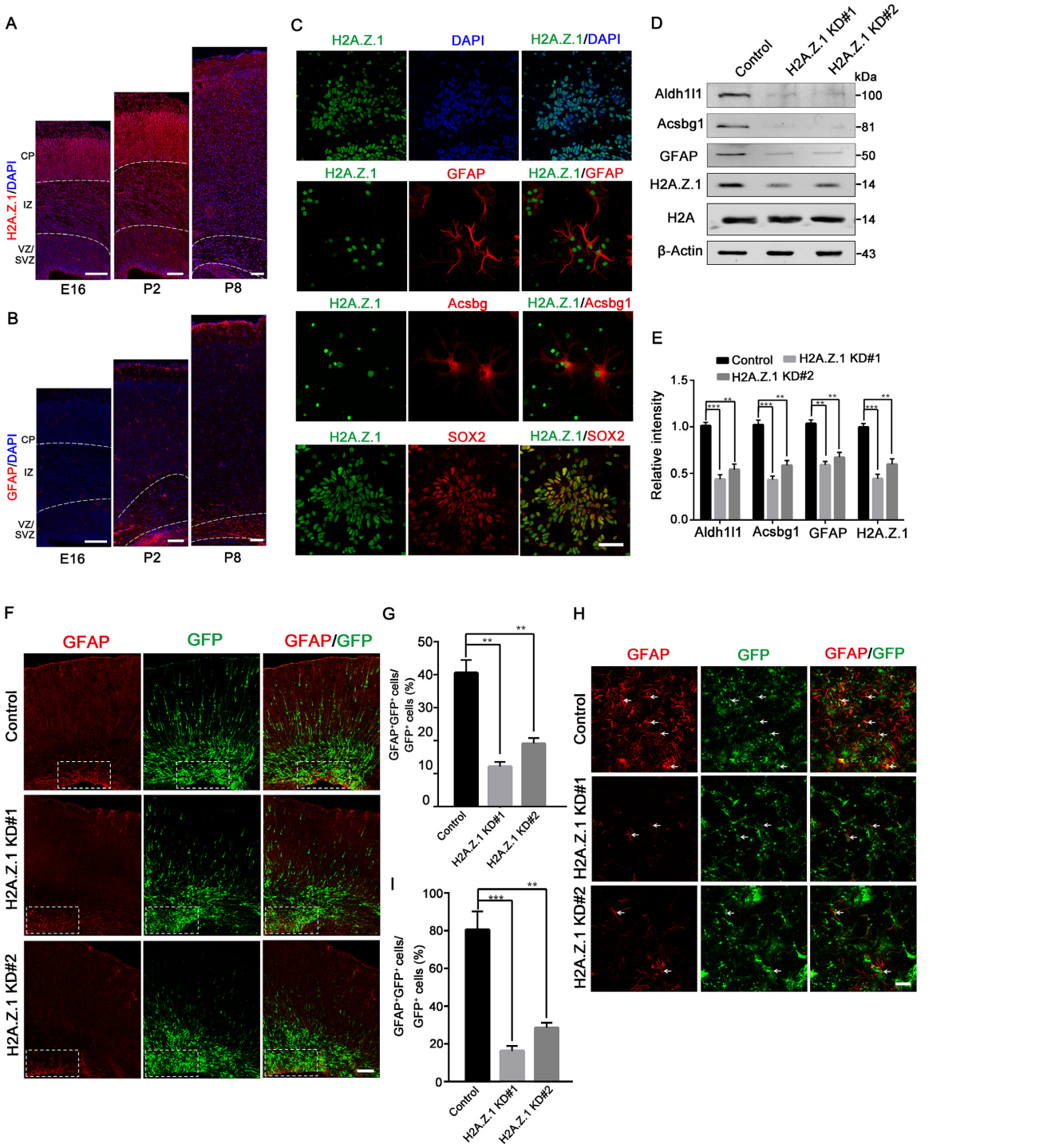

Figure 1. H2A.Z.1 regulates the differentiation of astrocytes *in vitro* and *in vivo.* (**A** and **B**) Immunofluorescence staining for GFAP and H2A.Z.1 in the cerebral cortex at E16.5, E18.5 and P8. Scale bar, 100 μm. (**C**) E16.5 NPCs were isolated from the mouse brain cortex and cultured for 1 or 3 days. Double staining for H2A.Z.1 and DAPI, GFAP, Acsbg1 or SOX2 in cultured cells. Scale bar, 50 μm. (**D**) E16.5 NPCs were infected with lentivirus encoding a control-shRNA (GFP) or a H2A.Z.1-shRNA (H2A.Z.1 KD#1; H2A.Z.1 KD#2) and then cultured in differentiation medium for 3 days. Western blot analysis for Aldh1l1, Acsbg1, GFAP, H2A.Z.1 and H2A expression in cultured NPCs. *H2A.Z.1* knockdown inhibits the differentiation of NPCs, while the classic H2A histones are not affected. (**E**) Quantifications of Aldh1l1, Acsbg1, GFAP and H2A.Z.1 expressions when *H2A.Z.1* was knocked down. Data are represented as means ± S.E.M. ($n = 3$; one-way ANOVA; $^{**}P < 0.01$, $^{***}P < 0.001$). (**F**) Control-shRNA or H2A.Z.1-shRNA plasmids were injected into the lateral ventricles of E15.5 embryonic brains and electroporated into the mouse cortex. The brains were isolated from newborns (P0) and subsequently immunostained with astrocyte marker GFAP. Scale bar, 100 μm. (**G**) In the electroporated brain slices, the percentages of $GFAP^+GFP^+$ cells among the total GFP-positive cells. Data are represented as means ± S.E.M. ($n = 3$; one-way ANOVA; $^{**}P < 0.01$, $^{***}P < 0.001$). (**H**) E16.5 NPCs were infected with lentivirus encoding a control-shRNA or a H2A.Z.1-shRNA and then cultured in differentiation medium for 3 days. The cultured astrocytes were immunostained for GFAP. Scale bar, 100 μm. (**I**) In the NPCs cultures, the percentages of $GFAP^+GFP^+$ cells among the total GFP-positive cells. Data are represented as means ± S.E.M. ($n = 3$; one-way ANOVA; $^{**}P < 0.01$, $^{***}P < 0.001$).

and J). To further assess the function of H2A.Z.1 *in vivo*, the plasmids were electroporated into the E15.5 embryonic cortex, and brain sections were stained with the astrocyte marker GFAP. Results similar to the *in vitro* results were observed; the number of GFAP-labeled astrocytes among the GFP-positive cells was increased (Supplementary Figure S2K and L). What's more, the proportions of $Pax6^{+}$ cells decreased in the VZ/SVZ regions of H2A.Z.1 overexpression cortex (Supplementary Figure S2M). Additionally, glial progenitor proliferation and astrocyte differentiation were impaired during the late stage of the NPCs upon *H2A.Z.1* knockdown.

H2A.Z.1 deletion disrupts cortical gliogenesis during brain development

To further study the function of H2A.Z.1 in cortical gliogenesis, we used *H2A.Z.1* conditional knockout ($H2A.Z.1^{cKO}$) mice to examine the effect of H2A.Z.1. To generate $H2A.Z.1^{cKO}$ mice, we bred $H2A.Z.1^{fl/fl}$ mice with *hGFAP-Cre* mice (Figure 2A). To confirm the depletion of the *H2AFZ* gene in the $H2A.Z.1^{cKO}$ mouse brains, the expression levels of H2A.Z.1 at different stages (P2 and P8) were examined, and the results revealed that H2A.Z.1 expression was reduced (Figure 2B). Immunostaining of H2A.Z.1 at P8 also revealed a dramatic reduction in H2A.Z.1 expression (Supplementary Figure S3H). We also examined the expression levels of H2A.Z.1 at different organs between the $H2A.Z.1^{fl/fl}$ and $H2A.Z.1^{cKO}$ mouse. The expression levels of H2A.Z.1 at different organs were not affected except the brain (Supplementary Figure S3C). To confirm the glia progenitors had not been affected before gliogenesis, western blot analyses were performed using the different markers Sox2 and Pax6. There were no differences between the $H2A.Z.1^{fl/fl}$ and $H2A.Z.1^{cKO}$ mouse brain at different stages (Supplementary Figure S3D and E). Next, we examined the phenotypes of the $H2A.Z.1^{cKO}$ mice. Compared with the $H2A.Z.1^{fl/fl}$ mice, the $H2A.Z.1^{cKO}$ mice exhibited decreased brain sizes at P0 and P8 (Figure 2C and Supplementary Figure S3A). These results indicated that H2A.Z.1 is necessary for brain development. In addition to the previous facts, we also observed a reduced expression of the astrocyte marker GFAP in the $H2A.Z.1^{cKO}$ brains at P2 (Figure 2D and E). To further confirm the phenotypes, we also used a *Nestin-Cre* line mouse to conditionally knock out *H2A.Z.1*. Similar results were obtained in the *Nestin-Cre*/ *H2A.Z.1* cKO line mouse by western blot analysis. We also performed a terminal deoxynucleotidyltransferase-mediated dUTP end-labeling (TUNEL) assay to assess cells apoptosis. No significant difference was observed between the $H2A.Z.1^{fl/fl}$ and $H2A.Z.1^{cKO}$ brains, which suggested that the decrease in astrocytes in the $H2A.Z.1^{cKO}$ brains did not result from apoptotic cell death (Supplementary Figure S3F and G). To explore whether cortical astrocytogenesis was persistently influenced by *H2A.Z.1* deletion, we isolated the mouse brains at P8 and immunostained the brain sections with the astrocyte markers GFAP and S100β (40). The data revealed that the GFAP- and S100β-positive astrocyte numbers were reduced by 85.2% and 63.2%, respectively (Figure 2F and G). Western blot analysis also confirmed significant decreases in the astrocyte-specific proteins Aldh1l1, Acsbg1 and GFAP at the different stages of P2 and P8 (Figure 2H). Moreover, qPCR analysis also produced similar results (Supplementary Figure S3B). We also performed immunostaining with the astrocyte precursor markers GLAST and BLBP (41) at P0 and observed a slight decrease in astrocyte precursors (Supplementary Figure S3I and J). To further assess the cellular morphologies in the mutant cortex, we electroporated a GFP expression vector at P1 and analyzed the results at P8. The astrocytes of the mutant cortex exhibited an abnormal morphology that failed to elaborate extensive processes (Figure 2I). Taken together, our data suggest that H2A.Z.1 is necessary for glial progenitor specification and maintains the typical morphology of astrocytes.

H2A.Z.1 deletion impairs gliogenic signaling during gliogenesis

To explore the mechanisms by which H2A.Z.1 regulates glial progenitor specification, we performed *in vitro* culture experiments. Previous studies have demonstrated that the cytokine LIF is critical for astrocyte differentiation (12). E16.5 NPCs were treated with LIF in differentiation media for 2, 4 or 6 days. GFAP-positive astrocytes were induced by LIF as detected by western blotting and immunocytochemistry (Supplementary Figure S4A and B). The immunostaining for GFAP demonstrated that 8% of the cells differentiated into astrocytes in the $H2A.Z.1^{fl/fl}$ cultures without LIF treatment, whereas the astrocyte differentiation increased to 32% with LIF treatment. In the $H2A.Z.1^{cKO}$ cultures, merely 3.4% of the cells differentiated into GFAP-positive astrocytes without LIF treatment and the percentage of GFAP-positive cells increased to 9.1% after stimulation with LIF (Figure 3A and B). H2A.Z.1 exerted similar effects on NPC differentiation. The data revealed that the GFAP expression levels were dramatically reduced in the $H2A.Z.1^{cKO}$ cultures, whereas the neuronal marker βIII-tubulin (TUJ1) was not affected when compared to the $H2A.Z.1^{fl/fl}$ cultures (Figure 3C and D). Given that the heterodimerization of receptors leads to tyrosine phosphorylation by JAK tyrosine kinases, the tyrosine 705 site (Tyr^{705}) phosphorylation of STAT3 is critical for glial progenitor differentiation into astrocytes (13,42). To test whether the JAK–STAT pathway was impaired in the $H2A.Z.1^{cKO}$ cultures, cells were pre-treated with LIF (125 ng/ml) for 30 min before analysis by western blotting. The data demonstrated that the STAT3 phosphorylation level of Tyr^{705} was dramatically reduced in the $H2A.Z.1^{cKO}$ cultures, and LIF failed to induce the differentiation of glial progenitors during cortical development (Figure 3E and F). These data indicate that H2A.Z.1 regulates gliogenesis through the JAK–STAT pathway in the developing cortex.

H2A.Z.1 binds to anti-silencing function 1 a (ASF1a) and promotes H3K56 acetylation

In further study of the mechanism by which H2A.Z.1 influences astrocytogenesis, we tested whether there was a close relationship between H2A.Z.1 and histone modification. Given that H2A.Z.1 is always associated with the gene transcription, we examined some histone modification markers, including H3K56ac, H3K9ac, H3K27ac, H3K4me3

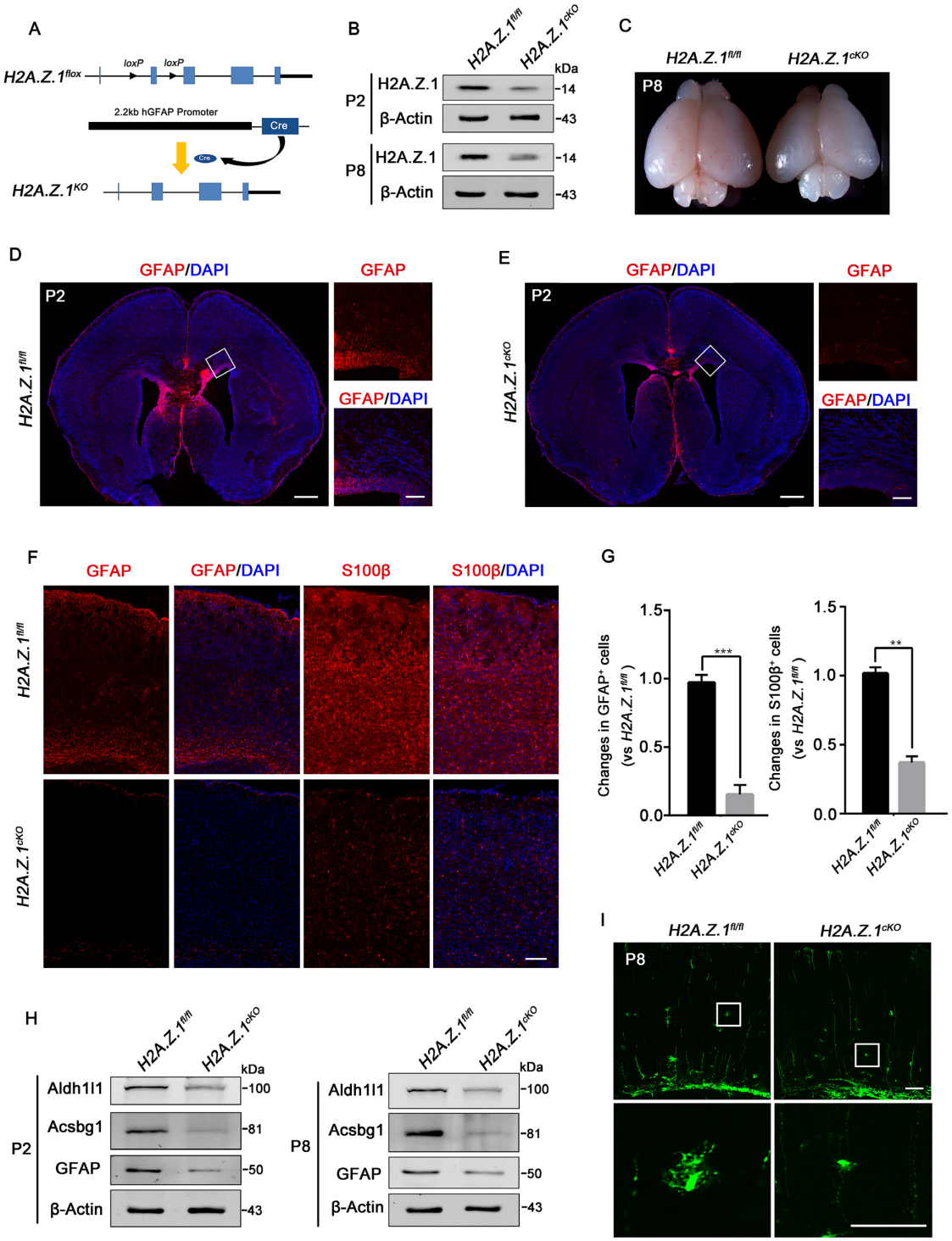

Figure 2. *H2A.Z.1* deletion disrupts glial progenitor specification during brain development. (**A**) Schematic of the *H2A.Z.1* knockout mouse construction strategy. The *H2AFZ* gene was knocked out by tissue-specific Cre recombinase splicing. (**B**) Western blot analysis of the H2A.Z.1 expression levels in the $H2A.Z.1^{fl/fl}$ and $H2A.Z.1^{cKO}$ cortices at P2 and P8. (**C**) Representative images of the $H2A.Z.1^{fl/fl}$ and $H2A.Z.1^{cKO}$ brain sizes at P8. The whole brains of the $H2A.Z.1^{cKO}$ are smaller than those of the $H2A.Z.1^{fl/fl}$ mice. Scale bar, 1 mm. (**D** and **E**) GFAP expression in $H2A.Z.1^{fl/fl}$ and $H2A.Z.1^{cKO}$ brain sections detected by immunofluorescence analysis at P2. The insets show high-magnification images of the delineated areas. Scale bars, 500 μm (left), 100 μm (right). (**F**) Confocal images of the GFAP and S100β expressions in the $H2A.Z.1^{fl/fl}$ and $H2A.Z.1^{cKO}$ cortices at P8. *H2AFZ* gene knockout also led to the persistent disruption of astrocyte number. Scale bar, 100 μm. (**G**) Quantification of the changes in the $GFAP^+$ and $S100\beta^+$ cells in the cortices of the $H2A.Z.1^{fl/fl}$ and $H2A.Z.1^{cKO}$ mice. Data are represented as means ± S.E.M. (n = 3; Student's *t*-test; $^{**}P < 0.01$, $^{***}P < 0.001$). (**H**) Western blot analysis of the astrocyte markers Aldh1l1, Acsbg1 and GFAP in the $H2A.Z.1^{cKO}$ and $H2A.Z.1^{fl/fl}$ cortices at stages P2 and P8. (**I**) Representative images of astrocyte morphology in the P8 cortex. The GFP plasmid was electroporated into the lateral ventricle of the P1 mouse brain. The astrocyte morphology was analyzed at P8. The GFP-labeled astrocytes did not exhibit typical astrocyte morphologies in the $H2A.Z.1^{cKO}$ cortices. The insets show high-magnification images of the delineated areas. Scale bars, 100 μm (top), 50 μm (bottom).

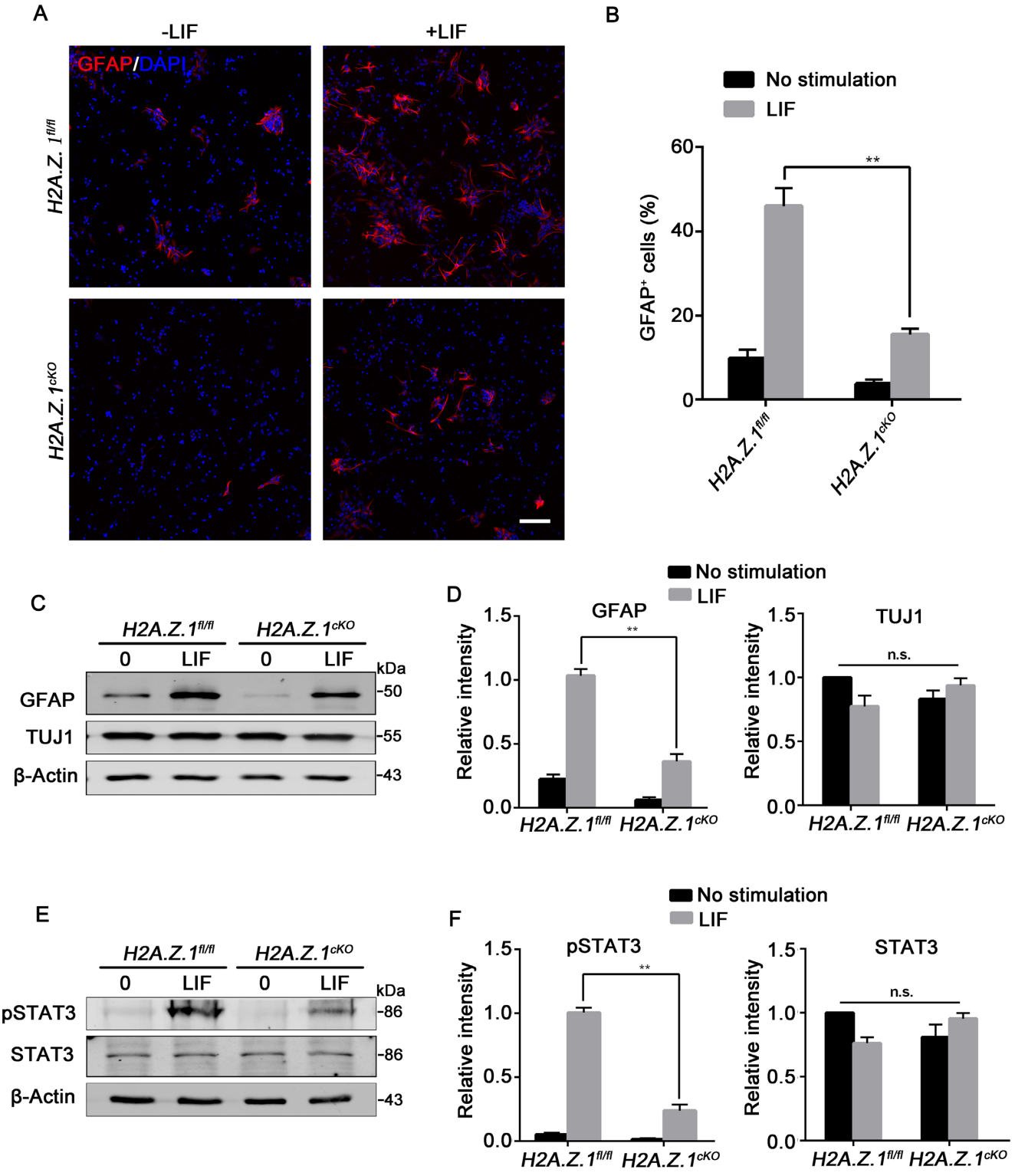

Figure 3. Gliogenic signaling is impaired in *in vitro* cultured NPCs. (**A**) Representative images of NPCs derived from E16.5 $H2A.Z.1^{fl/fl}$ and $H2A.Z.1^{cKO}$ cortices. NPCs were cultured in differentiation medium with or without LIF stimulation for 3 days before immunostaining for GFAP (red) and DAPI (blue). Scale bar, 100 μm. (**B**) Quantification of the percentage of $GFAP^+$ cells among the total cells after 3 days of culture. Data are represented as means ± S.E.M. (n = 3; Student's *t*-test; $^{**}P < 0.01$). (**C**) Western blot analysis of NPCs grown for 3 days with or without LIF (50 ng/ml) treatment. The GFAP expression was reduced, while the neural marker βIII-tubulin (TUJ1) was not affected in the mutant $H2A.Z.1^{cKO}$ cultures compared to the $H2A.Z.1^{fl/fl}$ cultures. (**D**) Quantifications of GFAP and βIII-tubulin expressions in wild-type and mutant progenitor cultures. Data are represented as means ± S.E.M. (n = 3; Student's t-test; $^{**}P < 0.01$). (**E**) Western blot analysis of NPCs with or without LIF (125 ng/ml) stimulation. The expression levels of phosphorylated STAT3 in the $H2A.Z.1^{cKO}$ mutant cultures were dramatically reduced when compared those in the $H2A.Z.1^{fl/fl}$ cultures, while the total STAT3 was not affected. Progenitor cultures pre-treated with LIF (125 ng/ml) for 30 min as indicated. (**F**) Quantifications of pSTAT3 and STAT3 expressions in wild-type and mutant progenitor cultures. Data are represented as means ± S.E.M. ($n = 3$; Student's *t*-test; $^{**}P < 0.01$).

and H3K36me3. Among these markers, H3K56ac was profoundly reduced, and the others exhibited no significant changes, after *H2A.Z.1* knockdown in NPCs (Figure 4A and B). Similar results were obtained in *H2A.Z.1*^{cKO} cortices by western blot analysis (Figure 4C and D).

ASF1a is a highly conserved chaperone of histones that is also related to acetylation. To test whether H2A.Z.1 physically interacted with ASF1a in the NPCs, we performed co-immunoprecipitation for Flag-H2A.Z.1 or Flag-H2A interaction with HA-ASF1a. The results revealed that H2A.Z.1 interacted with ASF1a (Figure 4E). To further confirm the physical interaction of endogenous H2A.Z.1 and ASF1a, the immunoprecipitated proteins were probed with endogenous H2A.Z.1 antibody. The endogenous Co-IP produced similar results. We also performed co-immunoprecipitation experiments to test the interactions between ASF1a with H3 or H2A. We did not observe obvious interactions between Asf1a with H3 or H2A, in our system (Figure 4F). Because ASF1a is required for acetylation and *H2A.Z.1* deletion impairs the level of H3K56 acetylation, we tested whether H2A.Z.1 and ASF1a play a collaborative role in regulating the acetylation of H3K56. When E16.5 NPCs were infected with H2A.Z.1 (or ASF1a) lentivirus, the pull down of H3K56ac was increased according to Co-IP analysis (Figure 4G and H). To further confirm the cooperative actions of H2A.Z.1 and ASF1a during the regulation of the H3K56ac level, NPCs were co-infected with H2A.Z.1-shRNA and ASF1a-shRNA lentiviruses. The H3K56 acetylation level was decreased (Figure 4I). Similarly, the level of H3K56ac was increased when H2A.Z.1 and ASF1a were co-expressed in NPCs (Figure 4J). Thus, we found that H2A.Z.1 cooperated with ASF1a in astrocyte specification and differentiation and the complex regulated the acetylation of H3K56 during gliogenesis.

Folate receptor 1 (FOLR1) is involved in cortical astrocytogenesis

To identify candidate downstream genes of H2A.Z.1 that function in astrocyte specification and differentiation, we performed RNA-seq to analyze the genome-wide changes. The RNA-seq data were derived from E16.5 *H2A.Z.1* deletion cortices. A volcano plots demonstrated that the transcripts of genes were differentially expressed between the wild-type and knockout cortices ($P < 0.01$, fold changes $>$ 2.0; Figure 5C). Gene Ontology (GO) analysis of the downregulated genes revealed a significant enrichment of biological processes related to NPCs differentiation that included regulation of cell differentiation and folic acid transport (Figure 5B). The upregulated genes exhibited a similar enrichment of biological processes according to the GO term analysis (Figure 5A). The GO term analysis indicated that H2A.Z.1 may play a critical role in cell differentiation and fate specification. After further analyzing the RNA-seq results, we noted a dramatic decrease in the expression of FOLR1 (Figure 5D), which is related to the development of the neural tube (43). Thus, FOLR1 is a promising candidate for a mediator of glial progenitor specification that acts through some cytokine signaling pathways. To confirm the downregulation of the *Folr1* gene, we validated the expression of FOLR1 in both *in vitro* cultured NPCs and *in vivo* cortical samples. Noticeably, there was a strong reduction in FOLR1 expression in the knockout and knockdown samples (Figure 5E). Further qPCR analysis validated the western blot analysis and demonstrated dramatic reductions upon *H2A.Z.1* depletion at the different stages of P2 and P8 (Supplementary Figure S5A and B).

Next, we sought to determine whether H2A.Z.1 is required for the regulation of the expression level of FOLR1 during cortex development. First, six different regions (from −5k to CDS) of the *Folr1* locus were designed for the enrichment analysis (Supplementary Figure S5C). We performed a chromatin immunoprecipitation analysis, and the results indicated that the H2A.Z.1 protein was significantly enriched in a region of the *Folr1* promoter surrounding position −2100 bp in the NPCs (Figure 5G). Given the fact that H2A.Z.1 interacted with ASF1a, we next sought to determine whether H2A.Z.1 regulates the expression of FOLR1 in collaboration with ASF1a. A ChIP analysis revealed that the ASF1a protein was highly enriched in the same region of the *Folr1* promoter (Supplementary Figure S5D). Furthermore, western blot analysis indicated that the expression level of FOLR1 was dramatically reduced. Conversely, the collaborative role of H2A.Z.1 and ASF1a promoted the expression of FOLR1 (Figure 5F). The data indicated that H2A.Z.1 and ASF1a co-occupied the core promoter regions of the *Folr1* gene. However, it is unknown whether H3K56ac is located in the promoter regions of the *Folr1* gene. We performed another ChIP analysis and found an enrichment of H3K56ac signals in the same surrounding position −2100 bp from the *Folr1* promoter (Figure 5H). To examine the functional relations between H2A.Z.1 and ASF1a, we also performed another ChIP analysis with H3K56ac antibodies. The results demonstrated that H2A.Z.1 interacts with ASF1a to promote the H3K56ac levels (Supplementary Figure S5E). Strikingly, H2A.Z.1 directly interacts with ASF1a to regulate the expression level of FOLR1 by altering the H3K56ac levels in the core promoter regions of the *Folr1* gene.

FOLR1 participates in gliogenesis through the JAK–STAT signaling pathway and rescues *H2A.Z.1*-depletion defects

Given the profound results that H2A.Z.1 regulates glial progenitor specification through the deregulation of FOLR1 expression, we asked whether *Folr1* depletion affects astrocyte differentiation during brain development. First, E16.5 NPCs that were infected with the shRNA lentivirus were examined, and the data indicated that *FOLR1* knockdown impaired astrocyte differentiation (Figure 6A and B). We also electroporated FOLR1-shRNAs into the E15.5 embryonic mouse cortices, and the brains were isolated at P0. The data revealed that the GFP$^+$ cells failed to differentiate into GFAP$^+$ astrocytes which resulted in phenotypes similar to that of the *H2A.Z.1* deletion (Figure 6D and E). The percentage of GFAP$^+$ astrocytes among the GFP$^+$ cells was decreased on *H2A.Z.1* depletion (Supplementary Figure S6A and B). These results substantiated the notion that FOLR1 participates in the process of gliogenesis both *in vitro* and *in vivo*. To further support these results, FOLR1 overexpression plasmids were electroporated into the E15.5 embryonic cortex, and brain sections were

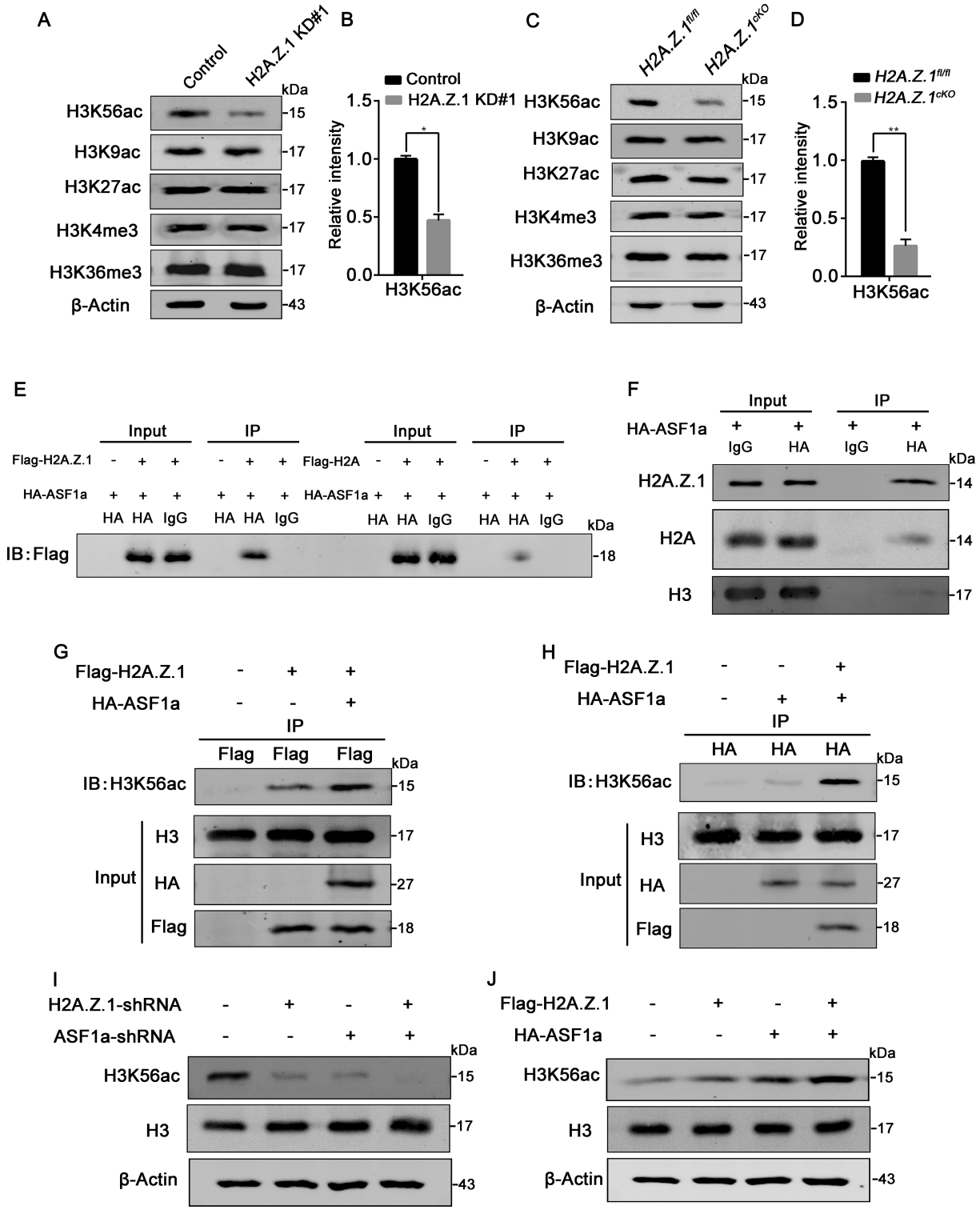

Figure 4. H2A.Z.1 directly and collaboratively interacts with ASF1a to regulate the acetylation of H3K56. (**A**) E15.5 NPCs were infected with a lentivirus encoding control-shRNA or H2A.Z.1-shRNA and cultured for 3 days. Western blot analyses of H3K56ac, H3K9ac, H3K27ac, H3K4me3 and H3K36me3 expressions in the cultured NPCs. (**B**) Quantification of H3K56ac expression in control and *H2A.Z.1* knockdown progenitor cultures. Data are represented as means ± S.E.M. ($n = 3$; Student's t-test; $^*P < 0.05$). (**C**) Western blot analyses of H3K56ac, H3K9ac, H3K27ac, H3K4me3 and H3K36me3 expression levels in the $H2A.Z.1^{fl/fl}$ and $H2A.Z.1^{cKO}$ cortices at P2. (**D**) Quantification of H3K56ac expression in the $H2A.Z.1^{fl/fl}$ and $H2A.Z.1^{cKO}$ cortices. Data are represented as means ± S.E.M. ($n = 3$; Student's *t*-test; $^{**}P < 0.01$). (**E**) Western blot of the co-immunoprecipitation of Flag-H2A.Z.1 or Flag-H2A interaction with HA-ASF1a. (**F**) H2A.Z.1 was immunoprecipitated by HA-ASF1a and detected endogenous H2A.Z.1, H2A or H3. Neuro2a cells were transfected with recombinant HA-ASF1a plasmids. (**G** and **H**) H2A.Z.1 and ASF1a promote the acetylation of H3K56ac in a collaborative manner. HA-ASF1a and Flag-H2A.Z.1 were co-expressed in the NPCs. (**I**) Western blot analyses of the H3K56ac expression levels when H2A.Z.1 or ASF1a was knocked down. (**J**) Western blot analyses of the H3K56ac expression levels when H2A.Z.1 or ASF1a was overexpressed.

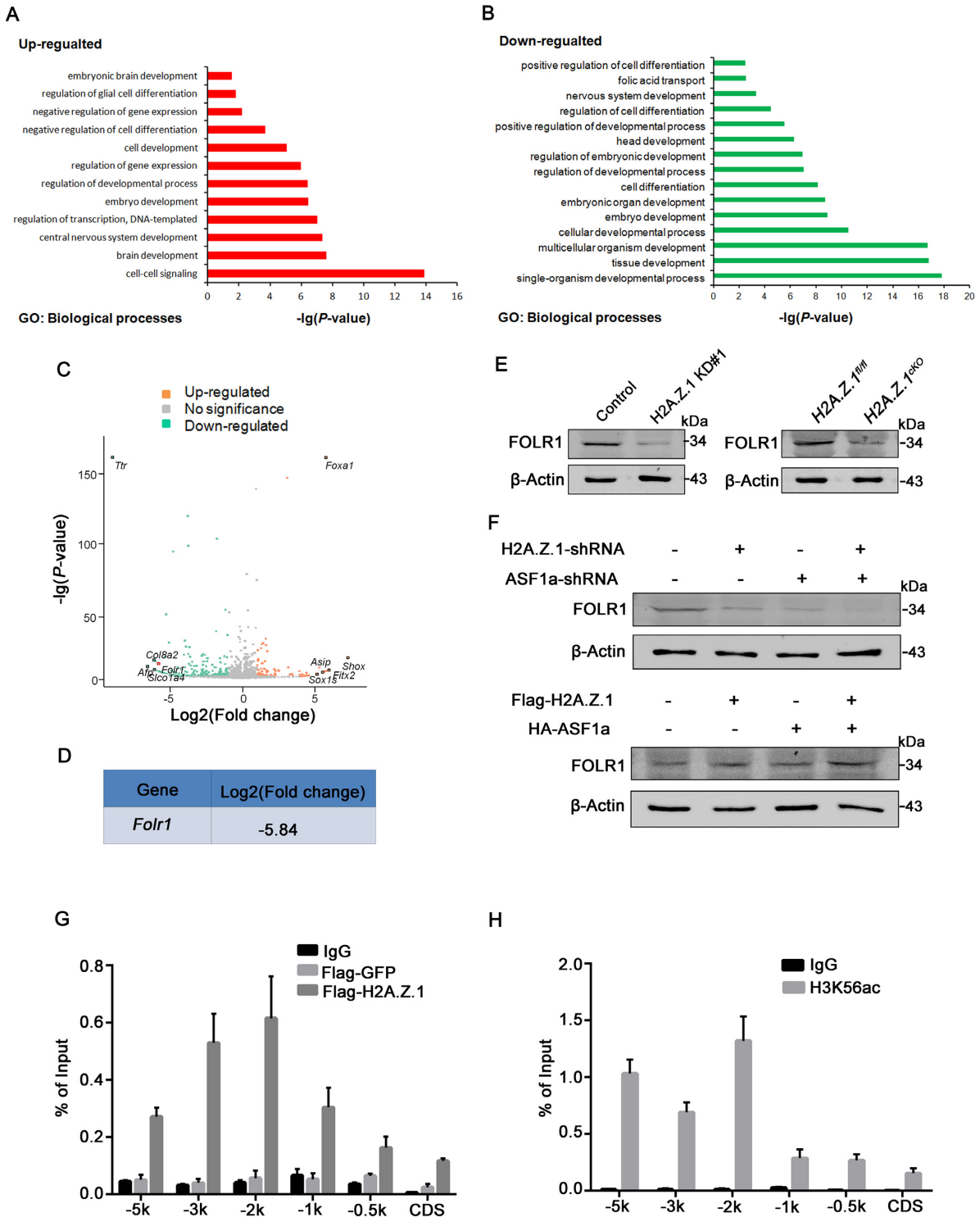

Figure 5. H2A.Z.1 regulates astrocyte differentiation of NPCs through FOLR1. (**A** and **B**) Enrichment analysis of the biological processes based on the RNA-seq results that indicated the downregulated and upregulated genes. The log(*P*-values) are indicated by the bar plots. (**C**) Volcano plots showing the gene profiling expression states. RNA-seq analysis showed the mRNAs with expression levels that were downregulated or upregulated by more than two-fold. Among the downregulated genes, the *Folr1* gene (red rim dot) was significantly reduced. (**D**) RNA-seq analysis showing that the *Folr1* mRNA expression level was dramatically reduced in the mutants. (**E**) Left: Western blotting confirmed the dramatic reduction in FOLR1 expression. Right: Western blot analyses of the FOLR1 expression levels in the *H2A.Z.1*$^{fl/fl}$ and *H2A.Z.1*^{cKO} cortices at P2. (**F**) Top: Western blot analyses of the FOLR1 expression levels when *H2A.Z.1* or *ASF1a* was knocked down. Bottom: Western blot analyses of the FOLR1 expression levels when H2A.Z.1 or ASF1a was overexpressed. (**G**) ChIP analysis revealed that H2A.Z.1 binds to the *Folr1* promoter region in NPCs. Primary NPCs were infected with control, Flag-GFP and Flag-H2A.Z.1 overexpression lentiviruses. Six different regions (from −5k to CDS) of the *Folr1* position were used for the analysis. Data are represented as means ± S.E.M. ($n = 3$). (**H**) qPCR results of the ChIP assay for H3K56ac binding to the region of the *Folr1* promoter in the NPCs. Data are represented as means ± S.E.M. ($n = 3$).

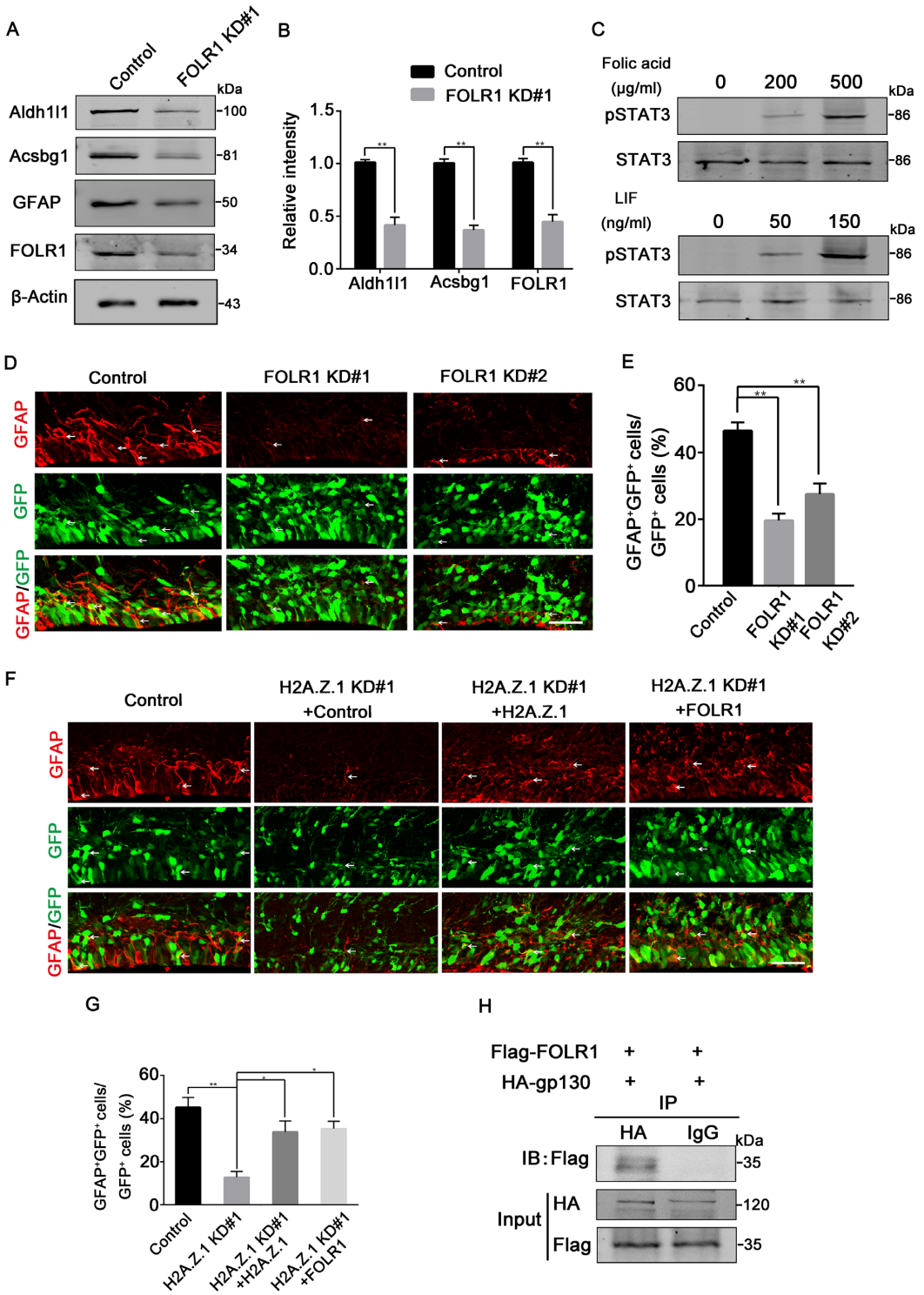

Figure 6. FOLR1 can rescue the deficiency that resulted from *H2A.Z.1* depletion. (**A**) Western blot analyses of Aldh1l1, Acsbg1, GFAP and FOLR1 expressions in cultured NPCs. (**B**) Quantifications of Aldh1l1, Acsbg1 and FOLR1 expressions when *Folr1* was knocked down. Data are represented as means ± S.E.M. ($n = 3$; Student's *t*-test; $^{**}P < 0.01$). (**C**) Western blot analysis of STAT3 activation by folic acid and LIF in NPCs. Primary E16.5 NPCs were cultured in differentiation medium with folic acid (0, 200, 500 μg/ml) or LIF (0, 50, 150 ng/ml) stimulation for 30 min. STAT3 was used as an endogenous control. (**D**) Plasmids were injected into the lateral ventricles of E15.5 embryonic brains. The brains were isolated at birth (P0) and subsequently immunostained with GFAP to label the astrocytes. Scale bar, 100 μm. (**E**) The percentages of $GFAP^+GFP^+$ cells among the total GFP-positive cells. Data are represented as means ± S.E.M. ($n = 3$; Student's *t*-test; $^{**}P < 0.01$). (**F**) The decrease in astrocyte number caused by *H2A.Z.1* knockdown is rescued by H2A.Z.1 or FOLR1. H2A.Z.1- or FOLR1-expressing plasmids were co-electroporated with H2A.Z.1-shRNA at E15.5. The brains were isolated at birth (P0) and subsequently immunostained with GFAP to label the astrocytes. (**G**) The percentages of $GFAP^+GFP^+$ cells among the total GFP-positive cells. Data are represented as means ± S.E.M. ($n = 3$; Student's *t*-test; $^{**}P < 0.01$, $^{*}P < 0.05$). (**H**) Western blot of the co-immunoprecipitation of gp130 and FOLR1.

stained with the astrocyte marker GFAP. The results revealed that the number of GFAP-labeled astrocytes among the GFP^+ cells was increased (Supplementary Figure S6C). We also overexpressed FOLR1 in NPCs at E16.5 and noted a major increase in astrocyte differentiation (Supplementary Figure S6D and E). We investigated the changes of NPCs proliferation *in vivo*. The data revealed that FOLR1 overexpression caused decreases in BrdU incorporation in the GFP-positive cells (Supplementary Figure S6F and G). We also performed a terminal deoxynucleotidyltransferase-mediated dUTP end-labeling (TUNEL) assay to assess cells apoptosis. There were no significant differences between the control cortex and the FOLR1 overexpression cortex (Supplementary Figure S6H). Next, we asked whether FOLR1 could rescue the phenotypes caused by *H2A.Z.1* deletion. We performed *in utero* electroporation to co-express H2A.Z.1-shRNA and FOLR1 in the mouse cortex. The data revealed that, the overexpression of FOLR1 partially rescue the defects of astrocyte differentiation caused by *H2A.Z.1* knockdown. Simultaneously, H2A.Z.1 overexpression also rescued the gliogenesis defects caused by *H2A.Z.1* silencing (Figure 6F and G). To further confirm the rescue by overexpressing FOLR1, E16.5 NPCs were co-infected with lentivirus and stained with the astrocyte marker GFAP. Consistently, the defects of astrocyte differentiation caused by *H2A.Z.1* knockdown were partially rescued by the overexpression of FOLR1 or H2A.Z.1 (Supplementary Figure S6I).

Because JAK–STAT signaling is the main pathway for gliogenesis and FOLR1 is a key receptor in the mediation of the transport of some cytokine signals, we test whether FOLR1 forms a receptor complex with other signal-transducing receptors, such as gp130, which is as a common receptor for LIF and other growth factors (44). NPCs were treated with different doses of folic acid for 30 min, and subsequent western blot analysis revealed that the expression level of pSTAT3 was increased by folic acid (Figure 6C). Next, we test whether FOLR1 interacts with gp130 as a co-receptor. We performed Co-IP assays and found that FOLR1 and gp130 directly interacted with each other (Figure 6H). To further confirm these results, the Flag-FOLR1 and HA-gp130 plasmids were co-transfected, and the results indicated that Flag- FOLR1 colocalized with HA-gp130 (Supplementary Figure S6J). Finally, we confirmed that STAT3 significantly increased the astrocyte differentiation and LIF stimulation further activated the JAK–STAT signaling pathway (Supplementary Figure S6K). Thus, we uncover a novel mechanism in which H2A.Z.1 regulates gliogenesis by affecting FOLR1 through the JAK–STAT signaling pathway.

DISCUSSION

During brain development, neurogenesis and gliogenesis follow an intrinsic developmental sequence. In the mouse brain, ventricular zone (VZ) progenitor cells develop prenatally into both neurons and glial cells (1,4). ventricular zone gliogenesis begins at E15 and plays an important role in embryonic cortex development (45). Astrocytes are thought to have many functions, including supplying metabolic support to neurons and aiding synapse formation (8,9). Many studies have focused on the neurogenesis, and increasing numbers of functions of astrocytes have been found in recent years (18,46). Nevertheless, astrocyte development, especially the specification step, requires further study to illuminate the molecular mechanisms and improve our understanding of brain diseases associated with astrocytes. In our study, we demonstrated that histone variant H2A.Z.1 crosstalk with the recently demonstrated chromatin marker H3K56ac acts to regulate gliogenesis in the developing cortex. Recently, a related study demonstrated that H2A.Z.1 regulates embryonic neurogenesis (27). As for the embryonic cortex development, neurogenesis and gliogenesis are inextricably intertwined. We focus on electroporation of H2A.Z.1-shRNAs at E15 for gliogenesis and H2A.Z knockdown decreases the astrocyte differentiation, while Shen et al. focus on electroporation of H2A.Z.1-shRNAs at E13 for neurogenesis. The two studies connect gliogenesis with neurogenesis in its entirety to understand the important role of H2A.Z.1 in embryonic cortex development.

Epigenetic regulation of normal brain function is involved in many processes including histone post-synthetic modifications and the incorporation of histone variants into nucleosomes (47). Among these processes, the incorporation of H2A.Z.1 into the nucleosomes has been linked to neural plasticity. Therefore, we hypothesize that H2A.Z.1 may regulate gliogenesis during brain development. To test this hypothesis, we first detected the expression of H2A.Z.1 and found that H2A.Z.1 co-localized with the astrocyte markers Acsbg1 and GFAP, which suggested a relationship with astrocyte differentiation (Figure 1A-C). Next, the function of H2A.Z.1 in gliogenesis was examined in H2A.Z.1-shRNA electroporated mice and conditional knockout mice. We observed that *H2A.Z.1* deletion led to a significant reduction in astrocyte number in the mutant cortex (Figures 1 and 2). Additionally, the *H2A.Z.1* knockout also resulted in a persistent disruption of the astrocyte number at P8. The typical astrocyte morphology is the basis of its various functions, and the astrocyte morphology was impaired in the $H2A.Z.1^{cKO}$cortices. The JAK–STAT signaling pathway is a major cytokine signaling cascade that promotes gliogenesis (13). Our findings indicated that the JAK–STAT pathway is impaired, and the phosphorylated STAT3 level was reduce decreased in the $H2A.Z.1^{cKO}$ cultures, which suggests that H2A.Z.1 regulates astrocyte differentiation through the JAK–STAT signaling pathway (Figure 3).

Histone modification is an important mechanism of regulating gene expression and the crosstalk between histone variants. H3K56ac is a recently demonstrated and relatively unstudied chromatin marker in mammalian cells that is related to memory formation in the hippocampus (33). More specifically, H2A.Z.1 and H3K56ac promote histone dynamics at promoters. This suggests a new pathway for how H2A.Z.1 promotes nucleosome dynamics (48). In the present work, we found that H3K56 acetylation is decreased when H2A.Z.1 is silenced. However, the relationship between H2A.Z.1 and H3K56 acetylation remained unclear. Here, we identified the highly conserved chaperone of histones H3/H4 anti-silencing function 1a (ASF1a). Interestingly, ASF1a is required for the maintenance of cellu-

lar reprogramming and interacts with Rtt109 to promote H3K56ac (49,50). Our results provide evidence that ASF1a is specifically required for H3K56 acetylation and thus influences the regulation of gene expression. Due to the ability of ASF1a to target H3K56ac, we tested the potential participation of ASF1a in astrocyte differentiation. We found that H2A.Z.1 directly cooperates with ASF1a to regulate the level of H3K56 acetylation (Figure 4E-J), which in turn controls astrocyte differentiation. The collaborative role between H2A.Z.1 and ASF1a provides a new view of the regulation of H3K56 acetylation in the CNS.

We also found that H2A.Z.1 regulates astrocyte differentiation through the JAK–STAT signaling pathway. GO analysis of the RNA-seq results demonstrated that the downregulated genes exhibited significant enrichment in cell fate commitment. Via further analysis, we found that FOLR1, a folic acid transporter and receptor, was dramatically reduced upon *H2A.Z.1* depletion (Figure 5). Additionally, we performed a qPCR-ChIP analysis to confirm that H2A.Z.1 could bind to the promoter of *Folr1*. To examine the H3K56ac levels, we also performed a ChIP analysis in the NPCs and observed an enrichment of H3K56ac in the same region of the *Folr1* promoter. Previous studies have demonstrated that the JAK–STAT signaling pathway is important for astrocyte differentiation (42). Many factors cooperate with the JAK–STAT signaling pathway to regulate astrocyte formation. Therefore, we examined that FOLR1 may participate in gliogenesis through the JAK–STAT signaling pathway. Given that FOLR1 is attached to the cell surface, FOLR1 may interact with other receptors in the JAK–STAT signaling pathway. It is known that gp130 is a signal-transducing component in receptor complexes that induce the differentiation of astrocytes (14). We next tested the interaction of FOLR1 and gp130 (Figure 6H). We found that FOLR1 interacted with gp130 as a component of a co-receptor that mediates signaling in the JAK–STAT signaling pathway. Finally, the co-localization supports the fact that FOLR1 indeed interacts with gp130. These results demonstrate that FOLR1 acts as a component of a co-receptor in the JAK–STAT signaling pathway during cortex gliogenesis.

DATA AVAILABILITY

RNA-seq accession codes: All sequencing-derived data reported in this study have been deposited in NCBI's Gene Expression Omnibus (GEO) under accession number GSE101939. The RNA-seq analyses had been linked to UCSC genome browser session. The link is: http://genome.ucsc.edu/cgi-bin/hgTracks?hgS_doOtherUser=submit&hgS_otherUserName=jwjiao&hgS_otherUserSessionName=H2ZKO_E16_WT_E16

SUPPLEMENTARY DATA

Supplementary Data are available at NAR Online.

ACKNOWLEDGEMENTS

We thank L.S., W.X. and J.J. designed and conceptualized the research; L.S. performed the experiments and analyzed the data; W.X. performed some of the IUE and discussed results; T.S. and Q.L. provided technical assistance and some plasmids; W.W. provided some assistance about our experiences; H.L. offered advice about our experiences; L.S. wrote the manuscript; J.J. supervised the project and obtained funding support.

FUNDING

CAS Strategic Priority Research Program [XDA16020602]; National Natural Science Foundation of China [31730033 and 31621004]; National Key Basic Research Program of China [2015CB964500 and 2014CB964903]; K.C. Wong Education Foundation. Funding for open access charge: CAS Strategic Priority Research Program [XDA16020602]; National Natural Science Foundation of China [31730033 and 31621004]; National Key Basic Research Program of China [2015CB964500 and 2014CB964903]; K.C. Wong Education Foundation.
Conflict of interest statement. None declared.

REFERENCES

1. Miller,F.D. and Gauthier,A.S. (2007) Timing is everything: Making neurons versus glia in the developing cortex. *Neuron*, **54**, 357–369.
2. Malatesta,P., Hack,M.A., Hartfuss,E., Kettenmann,H., Klinkert,W., Kirchhoff,F. and Gotz,M. (2003) Neuronal or glial progeny: regional differences in radial glia fate. *Neuron*, **37**, 751–764.
3. Haubensak,W., Attardo,A., Denk,W. and Huttner,W.B. (2004) Neurons arise in the basal neuroepithelium of the early mammalian telencephalon: a major site of neurogenesis. *PNAS*, **101**, 3196–3201.
4. Ge,W.P., Miyawaki,A., Gage,F.H., Jan,Y.N. and Jan,L.Y. (2012) Local generation of glia is a major astrocyte source in postnatal cortex. *Nature*, **484**, U376–U381.
5. Marshall,C.A., Suzuki,S.O. and Goldman,J.E. (2003) Gliogenic and neurogenic progenitors of the subventricular zone: who are they, where did they come from, and where are they going? *Glia*, **43**, 52–61.
6. Abbott,N.J., Ronnback,L. and Hansson,E. (2006) Astrocyte-endothelial interactions at the blood-brain barrier. *Nat. Rev. Neurosci.*, **7**, 41–53.
7. Koehler,R.C., Roman,R.J. and Harder,D.R. (2009) Astrocytes and the regulation of cerebral blood flow. *Trends Neurosci.*, **32**, 160–169.
8. Chung,W.S., Allen,N.J. and Eroglu,C. (2015) Astrocytes control synapse formation, function, and elimination. *Cold Spring Harb. Perspect. Biol.*, **7**, a020370.
9. Eroglu,C. and Barres,B.A. (2010) Regulation of synaptic connectivity by glia. *Nature*, **468**, 223–231.
10. Nedergaard,M., Ransom,B. and Goldman,S.A. (2003) New roles for astrocytes: redefining the functional architecture of the brain. *Trends Neurosci.*, **26**, 523–530.
11. Mertens,C. and Darnell,J.E. Jr. (2007) SnapShot: JAK–STAT signaling. *Cell*, **131**, 612.
12. Bonni,A., Sun,Y., Nadal-Vicens,M., Bhatt,A., Frank,D.A., Rozovsky,I., Stahl,N., Yancopoulos,G.D. and Greenberg,M.E. (1997) Regulation of gliogenesis in the central nervous system by the JAK–STAT signaling pathway. *Science*, **278**, 477–483.
13. Ceyzeriat,K., Abjean,L., Carrillo-de Sauvage,M.A., Ben Haim,L. and Escartin,C. (2016) The complex states of astrocyte reactivity: how are they controlled by the Jak-Stat3 pathway? *Neuroscience*, **330**, 205–218.
14. Nakashima,K., Wiese,S., Yanagisawa,M., Arakawa,H., Kimura,N., Hisatsune,T., Yoshida,K., Kishimoto,T., Sendtner,M. and Taga,T. (1999) Developmental requirement of gp130 signaling in neuronal survival and astrocyte differentiation. *J. Neurosci.*, **19**, 5429–5434.
15. Stahl,N., Boulton,T.G., Farruggella,T., Ip,N.Y., Davis,S., Witthuhn,B.A., Quelle,F.W., Silvennoinen,O., Barbieri,G., Pellegrini,S. *et al.* (1994) Association and activation of Jak-Tyk kinases by CNTF-LIF-OSM-IL-6 beta receptor components. *Science*, **263**, 92–95.

16. Taga,T. and Kishimoto,T. (1997) Gp130 and the interleukin-6 family of cytokines. *Annu. Rev. Immunol.*, **15**, 797–819.
17. Schwartzbaum,J.A., Fisher,J.L., Aldape,K.D. and Wrensch,M. (2006) Epidemiology and molecular pathology of glioma. *Nat. Clin. Pract. Neurol.*, **2**, 494–503.
18. Verkhratsky,A., Marutle,A., Rodriguez-Arellano,J.J. and Nordberg,A. (2015) Glial asthenia and functional paralysis: a new perspective on neurodegeneration and Alzheimer's disease. *Neuroscientist*, **21**, 552–568.
19. Zlatanova,J. and Thakar,A. (2008) H2A.Z: view from the top. *Structure*, **16**, 166–179.
20. Bargaje,R., Alam,M.P., Patowary,A., Sarkar,M., Ali,T., Gupta,S., Garg,M., Singh,M., Purkanti,R., Scaria,V. *et al.* (2012) Proximity of H2A.Z containing nucleosome to the transcription start site influences gene expression levels in the mammalian liver and brain. *Nucleic Acids Res.*, **40**, 8965–8978.
21. Bonisch,C. and Hake,S.B. (2012) Histone H2A variants in nucleosomes and chromatin: more or less stable? *Nucleic Acids Res.*, **40**, 10719–10741.
22. Faast,R., Thonglairoam,V., Schulz,T.C., Beall,J., Wells,J.R.E., Taylor,H., Matthaei,K., Rathjen,P.D., Tremethick,D.J. and Lyons,I. (2001) Histone variant H2A.Z is required for early mammalian development. *Curr. Biol.*, **11**, 1183–1187.
23. Draker,R., Ng,M.K., Sarcinella,E., Ignatchenko,V., Kislinger,T. and Cheung,P. (2012) A combination of H2A.Z and H4 acetylation recruits Brd2 to chromatin during transcriptional activation. *PLos Genet.*, **8**, e1003047.
24. Fan,J.Y., Rangasamy,D., Luger,K. and Tremethick,D.J. (2004) H2A.Z alters the nucleosome surface to promote HP1 alpha-mediated chromatin fiber folding. *Mol. Cell*, **16**, 655–661.
25. Maze,I., Noh,K.M., Soshnev,A.A. and Allis,C.D. (2014) Every amino acid matters: essential contributions of histone variants to mammalian development and disease. *Nat. Rev. Genet.*, **15**, 259–271.
26. Creyghton,M.P., Markoulaki,S., Levine,S.S., Hanna,J., Lodato,M.A., Sha,K., Young,R.A., Jaenisch,R. and Boyer,L.A. (2008) H2AZ Is enriched at polycomb complex target genes in ES cells and is necessary for lineage commitment. *Cell*, **135**, 649–661.
27. Shen,T., Ji,F., Wang,Y., Lei,X., Zhang,D. and Jiao,J. (2018) Brain-specific deletion of histone variant H2A.z results in cortical neurogenesis defects and neurodevelopmental disorder. *Nucleic Acids Res.*, **46**, 2290–2307.
28. Maze,I., Noh,K.M. and Allis,C.D. (2013) Histone regulation in the CNS: basic principles of epigenetic plasticity. *Neuropsychopharmacology*, **38**, 3–22.
29. Xie,W., Song,C.Y., Young,N.L., Sperling,A.S., Xu,F., Sridharan,R., Conway,A.E., Garcia,B.A., Plath,K., Clark,A.T. *et al.* (2009) Histone H3 lysine 56 acetylation is linked to the core transcriptional network in human embryonic stem cells. *Mol. Cell*, **33**, 417–427.
30. Williams,S.K., Truong,D. and Tyler,J.K. (2008) Acetylation in the globular core of histone H3 on lysine-56 promotes chromatin disassembly during transcriptional activation. *PNAS*, **105**, 9000–9005.
31. Li,Q., Zhou,H., Wurtele,H., Davies,B., Horazdovsky,B., Verreault,A. and Zhang,Z. (2008) Acetylation of histone H3 lysine 56 regulates replication-coupled nucleosome assembly. *Cell*, **134**, 244–255.
32. Yuan,J., Pu,M.T., Zhang,Z.G. and Lou,Z.K. (2009) Histone H3-K56 acetylation is important for genomic stability in mammals. *Cell Cycle*, **8**, 1747–1753.
33. Levenson,J.M., O'Riordan,K.J., Brown,K.D., Trinh,M.A., Molfese,D.L. and Sweatt,J.D. (2004) Regulation of histone acetylation during memory formation in the hippocampus. *J. Biol. Chem.*, **279**, 40545–40559.
34. Mohanty,V., Shah,A., Allender,E., Siddiqui,M.R., Monick,S., Ichi,S., Mania-Farnell,B., D,G.M., Tomita,T. and Mayanil,C.S. (2016) Folate Receptor Alpha Upregulates Oct4, Sox2 and Klf4 and Downregulates miR-138 and miR-let-7 in Cranial Neural Crest Cells. *Stem Cells*, **34**, 2721–2732.
35. Zhuo,L., Theis,M., Alvarez-Maya,I., Brenner,M., Willecke,K. and Messing,A. (2001) hGFAP-cre transgenic mice for manipulation of glial and neuronal function in vivo. *Genesis*, **31**, 85–94.
36. Wang,S.K., Li,B.G., Qiao,H.M., Lv,X.H., Liang,Q.L., Shi,Z.X., Xia,W.L., Ji,F. and Jiao,J.W. (2014) Autophagy-related gene Atg5 is essential for astrocyte differentiation in the developing mouse cortex. *EMBO Rep.*, **15**, 1053–1061.
37. Shen,T.J., Ji,F., Yuan,Z.Q. and Jiao,J.W. (2015) CHD2 is required for embryonic neurogenesis in the developing cerebral cortex. *Stem Cells*, **33**, 1794–1806.
38. Gao,Y., Chen,J., Li,K., Wu,T., Huang,B., Liu,W., Kou,X., Zhang,Y., Huang,H., Jiang,Y. *et al.* (2013) Replacement of Oct4 by Tet1 during iPSC induction reveals an important role of DNA methylation and hydroxymethylation in reprogramming. *Cell Stem Cell*, **12**, 453–469.
39. Cahoy,J.D., Emery,B., Kaushal,A., Foo,L.C., Zamanian,J.L., Christopherson,K.S., Xing,Y., Lubischer,J.L., Krieg,P.A., Krupenko,S.A. *et al.* (2008) A transcriptome database for astrocytes, neurons, and oligodendrocytes: a new resource for understanding brain development and function. *J. Neurosci.*, **28**, 264–278.
40. Rothstein,J.D., Martin,L., Levey,A.I., Dykes-Hoberg,M., Jin,L., Wu,D., Nash,N. and Kuncl,R.W. (1994) Localization of neuronal and glial glutamate transporters. *Neuron*, **13**, 713–725.
41. Campbell,K. and Gotz,M. (2002) Radial glia: multi-purpose cells for vertebrate brain development. *Trends Neurosci.*, **25**, 235–238.
42. He,F., Ge,W., Martinowich,K., Becker-Catania,S., Coskun,V., Zhu,W., Wu,H., Castro,D., Guillemot,F., Fan,G. *et al.* (2005) A positive autoregulatory loop of Jak-STAT signaling controls the onset of astrogliogenesis. *Nat. Neurosci.*, **8**, 616–625.
43. Wallingford,J.B., Niswander,L.A., Shaw,G.M. and Finnell,R.H. (2013) The continuing challenge of understanding, preventing, and treating neural tube defects. *Science*, **339**, 1222002.
44. Jenkins,B.J., Grail,D., Nheu,T., Najdovska,M., Wang,B., Waring,P., Inglese,M., McLoughlin,R.M., Jones,S.A., Topley,N. *et al.* (2005) Hyperactivation of Stat3 in gp130 mutant mice promotes gastric hyperproliferation and desensitizes TGF-beta signaling. *Nat. Med.*, **11**, 845–852.
45. Sauvageot,C.M. and Stiles,C.D. (2002) Molecular mechanisms controlling cortical gliogenesis. *Curr. Opin. Neurobiol.*, **12**, 244–249.
46. Nedergaard,M. (2013) Neuroscience. Garbage truck of the brain. *Science*, **340**, 1529–1530.
47. Sarma,K. and Reinberg,D. (2005) Histone variants meet their match. *Nat. Rev. Mol. Cell Biol.*, **6**, 139–149.
48. Watanabe,S., Radman-Livaja,M., Rando,O.J. and Peterson,C.L. (2013) A histone acetylation switch regulates H2A.Z deposition by the SWR-C remodeling enzyme. *Science*, **340**, 195–199.
49. Gonzalez-Munoz,E., Arboleda-Estudillo,Y., Otu,H.H. and Cibelli,J.B. (2014) Histone chaperone ASF1A is required for maintenance of pluripotency and cellular reprogramming. *Science*, **345**, 822–825.
50. Tsubota,T., Berndsen,C.E., Erkmann,J.A., Smith,C.L., Yang,L.H., Freitas,M.A., Denu,J.M. and Kaufman,P.D. (2007) Histone H3-K56 acetylation is catalyzed by histone chaperone-dependent complexes. *Mol. Cell*, **25**, 703–712.